THE JOURNAL OF PHYSICAL CHEMISTRY Letters

Letter

pubs.acs.org/JPCL

Role of Interlayer Coupling on the Evolution of Band Edges in Few-Layer Phosphorene

V. Wang,*[,†] Y. C. Liu,[‡,†] Y. Kawazoe,[¶,§] and W. T. Geng*[,∥]

[†]Department of Applied Physics, Xi'an University of Technology, Xi'an 710054, China

[‡]Department of Applied Physics, Xi'an Jiaotong University, Xi'an 710049, China

[¶]New Industry Creation Hatchery Center, Tohoku University, Sendai, Miyagi 980-8579, Japan

[§]Kutateladze Institute of Thermophysics, Siberian Branch of Russian Academy of Sciences, Novosibirsk 630090, Russia

[∥]School of Materials Science & Engineering, University of Science and Technology Beijing, Beijing 100083, China

Supporting Information

ABSTRACT: Using first-principles calculations, we have investigated the evolution of band edges in few-layer phosphorene as a function of the number of P layers. Our results predict that monolayer phosphorene is an indirect band gap semiconductor and its valence band edge is extremely sensitive to strain. Its band gap could undergo an indirect-to-direct transition under a lattice expansion as small as 1% along the zigzag direction. A semiempirical interlayer coupling model is proposed, which can reproduce the evolution of valence band edges obtained by first-principles calculations well. We conclude that the interlayer coupling plays a dominant role in the evolution of the band edges via decreasing both band gap and carrier effective masses with the increase of phosphorene thickness. Scrutiny of the orbital-decomposed band structure provides a better understanding of the upward shift of the valence band maximum, surpassing that of the conduction band minimum.

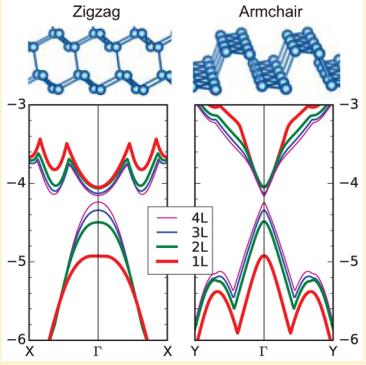

Recently, a novel two-dimensional material, few-layer black phosphorus (phosphorene), has been synthesized by the micromechanical exfoliation technique.[1,2] It arouses great interest of researchers due to many unparalleled properties superior to or not found in other members of the 2D materials family.[1−3] For example, it exhibits a carrier mobility up to 1000 $cm^2/V·s$ and an on/off ratio up to 10^4−10^5 for the phosphorene transistors at room temperature.[1,2,4] Its peculiar puckered honeycomb structure leads to significant anisotropic electronic and optical properties on zigzag and armchair directions.[5−8] Remarkably, the band gap of phosphorene is thickness-dependent, varying from 0.3 eV in the bulk limit to ∼2.2 eV in a monolayer with a direct band gap character.[1,2,7,9−18]

Although the structural, electronic, and optical properties of few-layer phosphorene have been extensively studied both experimentally and theoretically,[1,2,7,14−20] there are issues that remain controversial or even unexplored, to the best of our knowledge. For example, there is a debate on whether single-layer phosphorene could have a direct band gap.[21−25] Cai et al. attributed the thickness dependence of the band gap to the quantum confinement effect. Nevertheless, they noted that monolayer phosphorene is an exception.[26] Tran et al. predicted that the decay of the band gap of phosphorene with increasing thickness is significantly slower than the usual quantum confinement result.[15] This suggests that the quantum confinement effect alone is not enough to describe well the evolution of the band gap as a function of the number of P layers.[21−25] Another unresolved puzzle is that the upward shift of the valence band maximum (VBM) is faster than that of the conduction band minimum (CBM).[26,27] Obviously, our understanding of the thickness effect on the evolution of the band edges in phosphorene is still incomplete.

In this Letter, we attempt to answer these questions by examining the fine structure of band edges in few-layer phosphorene using first-principles calculations based on density functional theory (DFT).[28,29] Our results demonstrate that monolayer phosphorene has an indirect band gap and its valence band edge (VBE) is rather sensitive to the strain. A strain as small as 1% along the zigzag direction is enough to induce an indirect-to-direct band gap transition in monolayer phosphorene. On the basis of our first-principles results, we propose a semiempirical interlayer coupling (SEIC) model to interpret the evolution of the VBEs as a function of the P number of layers in few-layer phosphorene. This simple model can reproduce fairly well the evolution of VBEs determined by first-principles calculations, a strong indication that interlayer interaction is primarily responsible for the evolution of the band edges in few-layer phosphorene.

Our total energy and electronic structure calculations were performed using the Vienna ab initio simulation package (VASP).[30,31] The electron−ion interaction was described using

Received: September 15, 2015
Accepted: November 12, 2015
Published: November 18, 2015

DOI: 10.1021/acs.jpclett.5b02047
J. Phys. Chem. Lett. 2015, 6, 4876−4883

the projector augmented wave (PAW) method,[32,33] and the exchange and correlation were treated with generalized gradient approximation (GGA) in the Perdew Burke Ernzerhof (PBE) form.[34] It is well-known that the GGA method underestimates the semiconductor band gaps. However, in this study, we focused on the evolution of band edges in few-layer phosphorene; the band dispersions calculated by the GGA method exhibited similar features with the exception of the relative position of the valence and conduction bands when compared with the other higher-level methods, such as hybrid DFT or GW. We used a cutoff energy of 400 eV for the plane wave basis set, which yielded total energy convergences better than 1 meV/atom. Previous DFT calculations have shown that the interlayer van der Waals (vdW) interaction needs to be considered for a proper description of the geometrical properties of black phosphorus.[27,35] We therefore incorporated the vdW interactions by employing a semiempirical correction scheme of Grimme's DFT-D2 method in the following calculations, unless otherwise stated, which has been successful in describing the geometries of various layered materials.[36,37]

For the single-layer phosphorene, we also carried out local density approximation (LDA) using the Ceperley−Alder exchange−correlation potential as parametrized by Perdew and Zunger,[38] quasiparticle G0W0, and hybrid DFT[39−41] calculations for the purpose of comparison. To achieve good convergence of the dielectric function in the G0W0 calculations, we used a large number of bands (320) for the unit cell of the monolayer. The converged eigenvalues and wave functions, as well as the equilibrium geometry obtained from PBE functional, were chosen as the initial input for the G0W0 calculations. Note that in the G0W0 calculations, only the quasiparticle energies were recalculated self-consistently in one iteration; the wave functions were not updated but remained fixed at the PBE level. For visualization purpose, the G0W0 band structure was interpolated to a finer grid using an interpolation based on Wannier orbitals as implemented in the WANNIER90 code.[42] In the HSE06 approach, we here employed a revised scheme as proposed by Heyd, Scuseria, and Ernzerhof (HSE06).[43,44] Additional computational settings and a more detailed discussion of the ground-state properties were given in our previous DFT study of the native defect properties in phosphorene.[27]

In the slab model of few-layer phosphorene, periodic slabs were separated by a vacuum layer of 15 Å in the c direction to avoid mirror interactions. A 8 × 6 × 1 k-mesh including Γ-point, generated according to the Monkhorst−Pack scheme,[45] was applied to the Brillouin-zone integrations. Upon geometry optimization, both the shapes and internal structural parameters of pristine unit cells were fully relaxed until the residual force on each atom was less than 0.01 eV/Å. The fine structures of the band structures were calculated by sampling 301 k-points along each high-symmetry line in reciprocal space. The band structures and band edges were aligned with respect to the vacuum level which was determined by aligning the planar-averaged electrostatic potential in the vacuum region far from phosphorene layer. This provides a deeper intuitional insight into the physical origins of band edge evaluation. We used the VASPKIT code for postprocessing of the VASP calculated data.[46]

We begin by investigating the global band structure of monolayer phosphorene, aiming to find the locations of both VBM and CBM in the two-dimensional reciprocal lattice space. In Figure 1, we find that the band dispersion of VBE along the

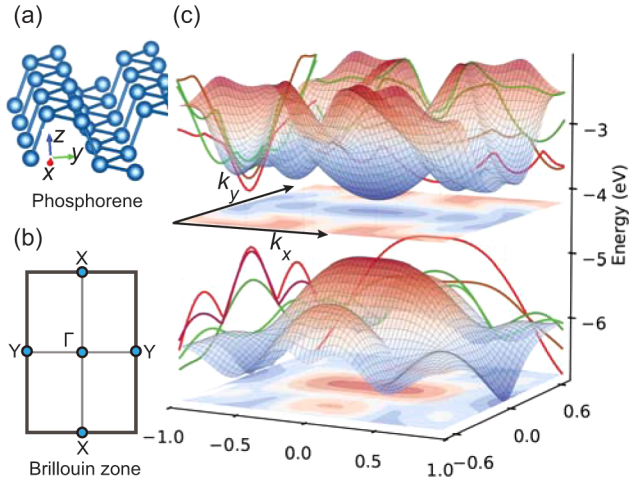

Figure 1. (a) Layered structure, (b) two-dimensional Brillouin zone, and (c) the highest valence and lowest conduction bands of monolayer phosphorene. Green and red curves are the projections of global band edges of the monolayer onto the xz and yz planes. The energy level of vacuum is set to zero.

wave vector k_y (corresponding to the armchair direction) near the high-symmetry Γ point is rather significant, implying a small effective mass of the hole carrier. In contrast, the band dispersion of the VBE along the wave vector k_x (the zigzag direction) is very flat, a signature of very heavy hole. A similar feature is also observed for the conduction band edge (CBE) dispersion. This means that highly anisotropic effective mass for both electron and hole carriers would be observed in monolayer phosphorene.[6] Meanwhile, it appears that both the VBM and CBM are located at the Γ point in the Brillouin zone, seemingly indicating that the monolayer has a direct band gap.

To gain further insights into the underlying physics, the orbital-projected band structure of the P atom ("fat bands") is shown in Figure 2. The band gap for monolayer phosphorene is predicted to be 0.91 eV by using the PBE approach. The lowest-lying valence bands are essentially s states, characterized by large dispersion along the Γ−X direction. Because the

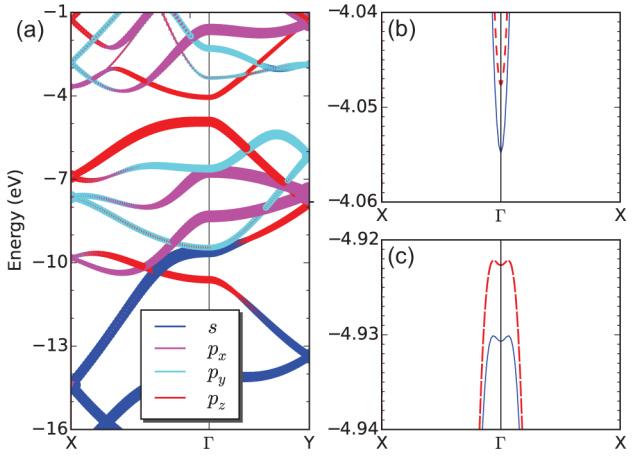

Figure 2. Orbital-projected band structure of monolayer phosphorene (a), and fine structures of CBE (b) and VBE (c) around the Γ point. The width of the line in (a) indicates the weight of the component. Blue solid and red dashed lines in (b) and (c) represent the band edges with and without spin−orbital coupling, respectively. The vacuum level is set to zero.

DOI: 10.1021/acs.jpclett.5b02047
J. Phys. Chem. Lett. 2015, 6, 4876−4883

variation of k_x has marginal effect on the p_y orbital, the bands consisting mainly of p_y states are relatively flat along the Γ−X direction. The opposite is true for the bands with p_x character in the Γ−Y direction. It is worth mentioning here that the p_x and p_y orbitals are not orthogonal to each other after hybridization. The VBE are mainly derived from the $\sigma-\sigma$ bonding states between p_z orbitals (weight percentage: 90.7%) in different P sublayers. For the CBE, the contributions of s (14.8%) and p_y (19.6%) become comparable with that of p_z (65.6%). Clearly, the interlayer interaction has a stronger effect on the p_z orbitals than on others. It is therefore expected that the position of the VBE is more sensitive to the number of P layers than that of CBE due to the interaction of p_z between neighboring P layers.

A closer view of the CBE and VBE are displayed in panels (b) and (c) of Figure 2, respectively. It is seen clearly that for monolayer phosphorene, the CBM is exactly located at the Γ point, but the VBM shifts slightly away from the Γ point by around $\pm 6.33 \times 10^{-2}$ Å^{-1} along the Γ−X direction. This means that monolayer phosphorene is not a direct band gap semiconductor. This special position is labeled as the Λ point, and its energy and position deviation from the Γ point are denoted as ΔE_Λ and Δk_Λ, respectively. On the basis of the **k·p** perturbation theory, Li et al. pointed out that the indirect band gap character of monolayer phosphorene originates from the coupling among s, p_y, and p_z orbitals because they have the same symmetry of Γ_2^+.[22] Our calculations show that the inclusion of spin−orbital coupling (SOC) shifts the VBE (CBE) toward (away from) the Fermi level by around 8 meV (7 meV). However, the relevant physics discussed above is not affected qualitatively. Thus, the SOC effect will not be considered in the following discussion.

For the purpose of comparison, we summarize in Table 1 the values of ΔE_Λ and Δk_Λ calculated using various methods with

Table 1. Calculated Lattice Constants *a* (Å, Zigzag Direction) and *b* (Å, Armchair Direction), P−P Bond Length *d* (Å), Energy and Location Deviation ΔE_Λ (meV), and Δk_Λ (Å^{-1}) of the Λ Point Away from the Γ Point in Monolayer Phosphorene, Using Various Methods Combined with/without the DFT-D2 Method

XC method	*a*	*b*	*d*	ΔE_Λ	Δk_Λ
LDA	3.27	4.38	2.20−2.23	12	±0.13
PBE	3.30	4.62	2.22−2.26	0.6	±0.06
PBE-D2	3.30	4.57	2.22−2.25	0.7	±0.06
HSE06-D2	3.27	4.53	2.19−2.22	99	±0.19
G0W0	3.30	4.57	2.22−2.25	11	±0.12

or without DFT-D2 correction. All methods predict that the monolayer phosphorene is not an exact direct gap semiconductor, in accordance with a recent GW work.[24] Most noticeably of all, the magnitude of ΔE_Λ yielded by the HSE06-D2 method even reaches ∼100 meV. We remind the reader that the calculated values of ΔE_Λ listed in Table 1 correspond to different equilibrium lattice constants. Further HSE06-D2 calculations using the optimal lattice constants obtained with PBE-D2 (LDA) give ΔE_Λ = 60 (93) meV and $\Delta k_\Lambda = \pm 0.15$ (0.16) Å^{-1}, respectively. Clearly, the magnitude of ΔE_Λ is sensitive to the P−P bond length. Because the PBE-D2 method still overestimates the lattice constants for bulk black phosphorus,[27] we speculate that the overestimation may extend to few-layer phosphorene. This might be a non-negligible factor to the very tiny value of ΔE_Λ. Moreover, LDA or GGA severely underestimates the semiconductor band gaps, and the HSE06 method is expected to yield more accurate ΔE_Λ for given lattice constants. In other words, the PBE method underestimates the energy difference between Λ and Γ when compared with the HSE06 result. Interestingly, we find that with a vacuum thickness of 25 Å, the G0W0 method gives values of ΔE_Λ and Δk_Λ very close to those of LDA. It is, however, worth mentioning that the G0W0-calculated band gaps are dependent on the vacuum thickness, as we shall demonstrate below. Unfortunately, no experimental data are available for comparison with the predicted values at present.

In view of the fact that GW calculations performed by different groups yield inconsistent band character of monolayer phophorene,[23−25] we also performed G0W0 calculations to examine the band structure of the monolayer as a function of vacuum thickness. We found that the band structure character of monolayer phosphorene, including both the band dispersion and band gap, is rather sensitive to the vacuum thickness. As seen in Figure 3a, the band dispersions of monolayer

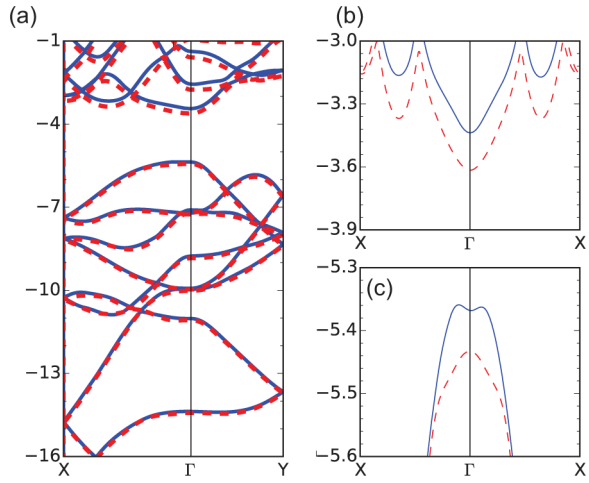

Figure 3. Band structure of monolayer phosphorene given by G0W0 (a) and fine structures of CBE (b) and VBE (c) around the Γ point. Blue and red lines represent the results of a slab model with a vacuum thickness of 25 and 15 Å, respectively. The vacuum level is set to zero.

configurations with different vacuum thicknesses (25 versus 15 Å) are qualitatively similar. However, they have different band characters when we look into the fine structure of VBE in Figure 3c. More specifically, with a vacuum thickness of 25 Å, G0W0 predicts an indirect band gap, in agreement with our PBE and HSE06 results. If we adopt a vacuum with a thickness of 15 Å in the slab model, G0W0 predicts a direct band gap. This sensitivity might be the reason for the discrepancy in previous G0W0 results reported in the literature. In addition, the gap value also varies linearly as a function of the inverse of the vacuum thickness (see Figure 4). Similar behavior was also found in other two-dimensional materials,[47,48] reflecting the long-range nature of the self-energy Σ = iGW.[48] Finally, the asymptotic gap value of 2.01 eV for monolayer phosphorene in the limiting case of infinite vacuum was obtained by an extrapolation scheme, very close to the recently reported experimental value of 2.2 eV.[7]

Next, we investigate the influence of lattice constants on the ΔE_Λ by applying uniform out-of-plane (ε_z) or in-plane strain to the unit cell of the mononlayer. The latter includes three cases,

DOI: 10.1021/acs.jpclett.5b02047
J. Phys. Chem. Lett. 2015, 6, 4876−4883

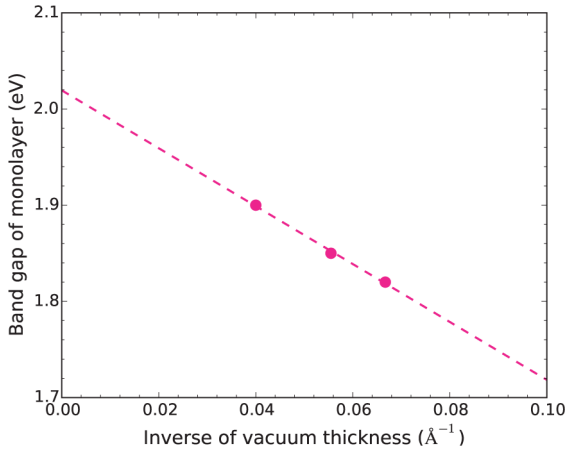

Figure 4. Band structure of monolayer phosphorene as a function of the inverse of vacuum thickness given by G0W0.

namely, the uniaxial strain along x (zigzag) or y (armchair) and the biaxial strain along both x and y directions, denoted by ε_x, ε_y, and ε_{xy}, respectively (see Figure 1). Taking the case of the uniaxial strain along the zigzag direction as an example, the applied strain is defined as $\varepsilon_x = \frac{a_x - a_{x0}}{a_{x0}}$, where a_x and a_{x0} are the lattice constants along the x direction for the strained and relaxed structures. A positive (negative) value of ε corresponds to a tensile (compressive) strain.

As seen in Figure 5, a uniform out-of-plane or in-plane compression lowers the eigenvalue at the Γ point. This leads to

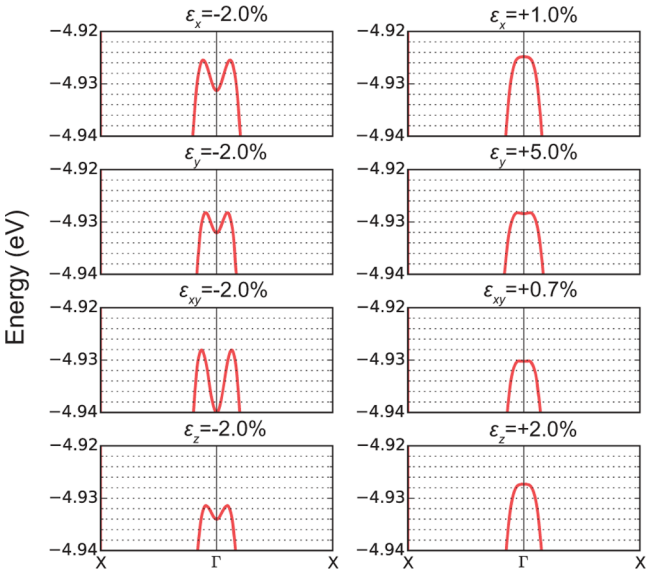

Figure 5. Evolution of VBE for monolayer phosphorene in response to strains determined by PBE-D2. For explanation of ε_x, ε_y, ε_z, and ε_{xy}, please see the text.

more significant indirect gap character of monolayer phosphorene. In contrast, the system undergoes a transition from indirect to direct band gap when tensile strains are applied. Our calculations predict that a small tensile strain of around 1% along the zigzag direction will induce such a transition. This implies that the band gap character of thin phosphorene films grown on different substrates could be different due to the introduction of strain by lattice mismatch. In contrast, the evolution of VBE is not sensitively dependent on the strain along the armchair direction. It is readily understandable if we consider the fact that the VBM is located at the Λ point in the Γ−X path (corresponding to the zigzag direction), as pointed out above. Previous first-principles calculations also showed that both the electronic and optical properties of single-layer phosphorene depend strongly on the applied strain.[49,50] To gain insight into such an observed trend in the VBE of monolayer phosphorene, we examine the bonding characters of the Γ point by plotting the band-decomposed electron density in Figure 6.

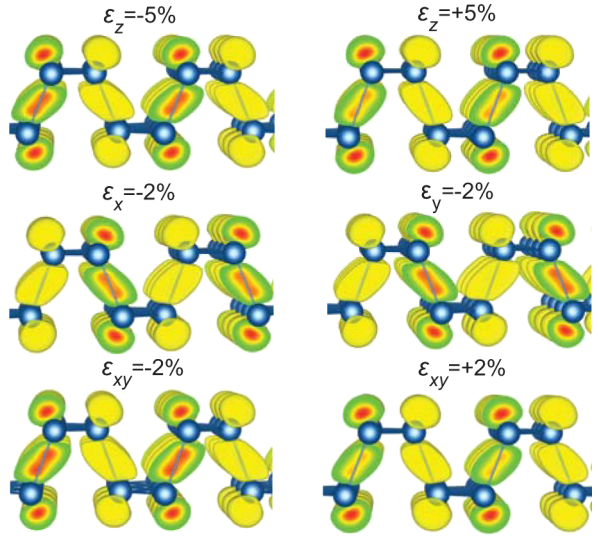

Figure 6. Charge density plots of the Γ point when monolayer phosphorene is subject to various strains. The isosurface is 0.01 e/Bohr^3.

We find that the depth of the concave-like shape of VBE near the Γ point is associated with the strength of ppσ bonding states between p_z orbitals of P atoms. More specifically, stronger bonding strength between p_z orbitals induces more significant indirect band gap character. Bonding strength can be enhanced by reducing the P−P bond length in different sublayers, that is, applying a compressive out-of-plane or in-plane strain. Phosphorus atoms have five electrons on 3p orbitals, three of which participate in the formation of three covalent σ-bonds with three neighboring P atoms by sp^3 hybridization in a puckered honeycomb structure and the remaining two electrons occupying a lone pair orbital oriented out-of-plane. Note that the magnitude of ΔE_Λ is more sensitive to in-plane strain than out-of-plane one. This means that the indirect gap character of VBE is also likely associated with the coulomb repulsion between electrons from the lone pair orbitals of neighboring P atoms.

When two or more isolated monolayers move close to each other to form multilayer phosphorene, the corresponding degenerate energy levels of different monolayers become nondegenerate due to the interlayer coupling, as shown in Figure 7. This leads to the splitting of the corresponding bands, which in turn push VBM and CBM to higher and lower energies, respectively. As a result, the magnitude of the band gap decreases with increasing the number of layers. On the basis of the careful analysis of the fine structure of conduction and valence bands, as shown in panels (b) and (c) of Figure 7, we conclude that bilayer phosphorene is a direct gap semiconductor. In other words, a transition from indirect to

DOI: 10.1021/acs.jpclett.5b02047
J. Phys. Chem. Lett. 2015, 6, 4876−4883

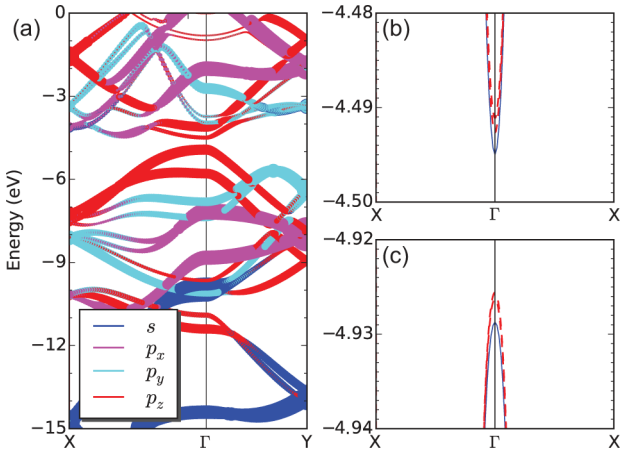

Figure 7. Orbital-projected band structure of bilayer phosphorene (a) and fine structures of CBE (b) and VBE (c) around the Γ point. The width of the line in (a) indicates the weight of the component. Blue solid and red dashed lines in (b) and (c) represent the band edges with and without SOC, respectively. The vacuum level is set to zero.

direct band gap occurs when going from the monolayer to bilayer.

Figures 8 and 9 show the evolution of band edges along the Γ−X and Γ−Y paths as a function of the number of P layers,

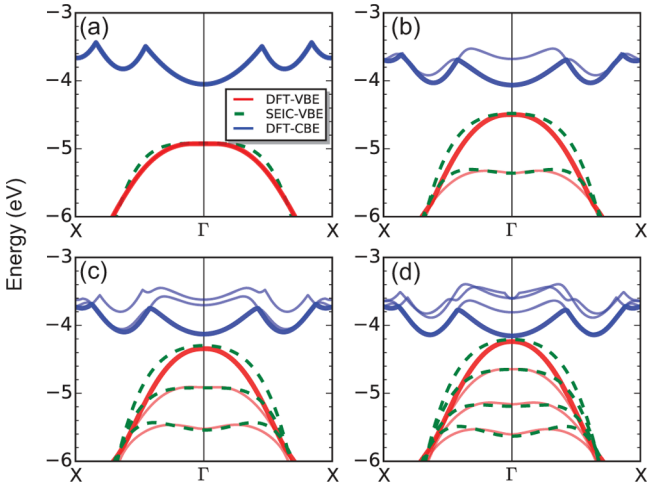

Figure 8. The evolution of the band edge states along the Γ−X direction as a function of the number of layers calculated by DFT and the SEIC model: (a) monolayer, (b) bilayer, (c) trilayer, and (d) quadrilayer. The vacuum level is set to zero.

respectively. One can find that the band dispersion of VBE along the Γ−X path becomes more significant with increasing film thickness due to the strong effect of interlayer coupling on the p_z orbital, suggesting that a significant decrease of hole carrier mass is to be observed with increasing the number of layers. Generally, a decrease in the carrier effective mass means an enhanced mobility. Therefore, few-layer phosphorene is likely to have better performance than monolayer phosphorene in electronic devices.

We find that the band dispersions of both VBE and CBE along the Γ−Y path change from a parabolic-like shape for the monolayer to a (nearly) linear-like shape for the quadrilayer, suggesting that the Dirac point observed in graphene could be also realized in few-layer phosphorene by tuning its band gap

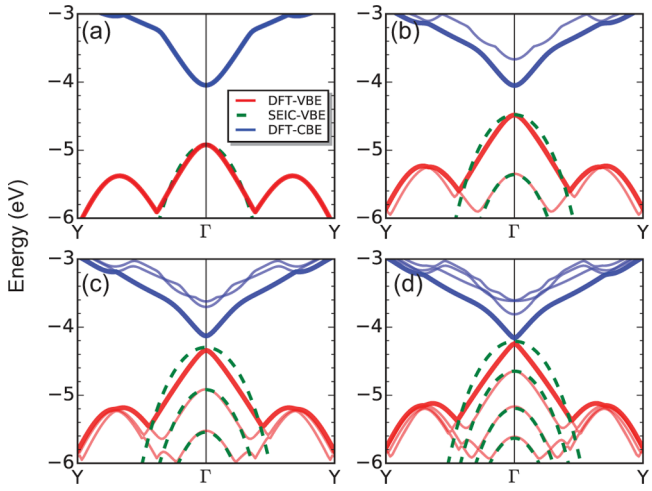

Figure 9. The evolution of the band edge states along the Γ−Y direction as a function of the number of layers calculated by DFT and the SEIC model: (a) monolayer, (b) bilayer, (c) trilayer, and (d) quadrilayer. The vacuum level is set to zero.

value to 0 eV. On the other hand, the VBE along the Γ−X direction remains a parabolic-like shape, indicating a significantly anisotropic band structure for the quadrilayer. We note a very recent experimental study that has reported that the tunable band gap and anisotropic Dirac semimetal state can be achieved by sprinkling potassium atoms on top of multilayer phosphorene.[51] Several recent theoretical studies also predicted that the Dirac cone in phosphorene can be achieved by application of an external electric field or strain.[52−54]

For the quadrilayer, it should be pointed out that the PBE method predicts a tiny gap value of around 0.1 eV, which is far smaller than the value of 0.71 (1.08) eV given by HSE06 (GW0).[27] Therefore, we attribute the linear dispersion of the quadrilayer to the strong interaction between the valence band and conduction band as a result of the severe gap underestimation by PBE. Further HSE06 calculations reveal that the band dispersion of the quadrilayer remains a parabolic-like shape but has a tendency toward linear dispersion when going from the monolayer to the bulk limit, as shown in Supporting Information Figure S1. It is found that the VBM shifts toward the Fermi level by 0.7 eV while the CBM shifts downward by 0.1 eV when going from the monolayer to the quadrilayer. The fact that the weight of p_z in VBE is larger than that in CBE is likely to be responsible for such observations. A similar trend has been found for MoS_2.[55] The global evolution of both the VBE and CBE for bilayer, trilayer, and quadrilayer systems is depicted in Supporting Information Figure S2.

It is now clear that the behavior of VBE is crucial for the electronic properties of phosphorene systems. Thus, we take the case of the VBE as an example and propose a SEIC model to describe the evolution of the VBE as a function of the number of P layers. As an extended Hückel molecular orbital theory,[56] the SEIC model can describe the interlayer interaction in layered materials. In this model, a multilayer phosphorene is seen as a "molecule", a monolayer is taken as an "atom", the energy bands in a monolayer are analogues of electron orbitals, and the interlayer coupling is the hybridization of the orbitals originating from different "atom" with the same symmetry. On the basis of **k·p** perturbation theory,[22] the band dispersion of the VBE near the Γ point in a monolayer can be approximately expressed as

DOI: 10.1021/acs.jpclett.5b02047
J. Phys. Chem. Lett. 2015, 6, 4876−4883

$$E_{1\nu}(k_x, k_y) = H_{1\nu}(k_x, k_y) = \varepsilon_0 + \alpha_x k_x^2 + \beta_x k_x^4 + \alpha_y k_y^2 + \beta_y k_y^4 \quad (1)$$

where $\varepsilon_0 = -4.92$ eV is the eigenvalue of the Γ point of the monolayer. The parameters α_x, α_y, β_x, and β_y are 0.04 eV·Å^2, −30.0 eV·Å^2, −80.0 eV·Å^4, and −100.0 eV·Å^4, respectively, indicating the anisotropic electronic properties on the zigzag and armchair directions. These values can be obtained by fitting the DFT-calculated band dispersion of the VBE for monolayer phosphorene. Here, k_x and k_y are given in units of $2\pi/a$ and $2\pi/b$, respectively, where a and b are the corresponding equilibrium lattice constants of few-layer phosphorene systems. Because we focus only on the interpretation for the evolution of the valence band edges along zigzag ($k_y = 0$) and armchair ($k_x = 0$) directions of few-layer phosphorene, the contribution of coupling between k_x and k_y to the valence band dispersions is neglected.

As for the multilayer, the interlayer interaction is described by a coupling term of $J_\nu(\mathbf{k})$. For simplicity, the interaction between non-neighboring layers is neglected without loss of accuracy. In the case of the VBE, the coupling of p_z−p_z orbitals in nearest-neighboring layers is only considered because the VBE is mainly derived from the p_z state, as pointed out above. Then, the interlayer coupling term of the VBE is defined as

$$J_\nu(k_x, k_y) = \mu + \nu_x k_x^2 + \nu_y k_y^2 \quad (2)$$

where μ, ν_x, and ν_y are the coupling parameters.

The Hamiltonian of valence band dispersions near the Γ point in the bilayer is

$$H_{2\nu}(k_x, k_y) = \begin{bmatrix} H_{1\nu} & J_\nu \\ J_\nu & H_{1\nu} \end{bmatrix} \quad (3)$$

and the eigenvalues of eq 3 are

$$E_{2\nu}^{\pm}(k_x, k_y) = E_{1\nu}(k_x, k_y) \pm J_\nu(k_x, k_y) \quad (4)$$

On the basis of the DFT-calculated results of valence band dispersions for the bilayer as displayed in Figure 8b, the parameters μ, ν_x, and ν_y are 0.44 eV, −4.18 eV·Å^2, and 6.0 eV·Å^2, respectively. One can find that the energy of the first and second highest valence bands of the bilayer is shifted upward and downward, respectively, by $J_\nu(k_x,k_y)$ eV, with respect to the monolayer. Note that $J_\nu(k_x,k_y)$ is wave-vector-dependent and reaches its maximum $\mu = 0.44$ eV at the Γ point. Clearly, our SEIC model reproduces the indirect−direct band gap transition when going from the monolayer to bilayer, as predicted by our DFT results. Next, we take the trilayer as an example to study the role of interlayer coupling on the evolution of VBE in a multilayer system. The Hamiltonian of the trilayer and the corresponding eigenvalues can be described as

$$H_{3\nu}(k_x, k_y) = \begin{bmatrix} H_{1\nu} & J_\nu & 0 \\ J_\nu & H_{1\nu} & J_\nu \\ 0 & J_\nu & H_{1\nu} \end{bmatrix} \quad (5)$$

and

$$E_{3\nu}^1(k_x, k_y) = E_{1\nu}(k_x, k_y) - \sqrt{2}J_\nu(k_x, k_y)$$
$$E_{3\nu}^2(k_x, k_y) = E_{1\nu}(k_x, k_y)$$
$$E_{3\nu}^3(k_x, k_y) = E_{1\nu}(k_x, k_y) + \sqrt{2}J_\nu(k_x, k_y) \quad (6)$$

The analysis is similar for the systems with more layers. For the n-layer system, the evolution of its VBE is determined by $E_{n\nu}(k_x,k_y) = E_{1\nu} + 2J_\nu\cdot\cos\frac{k}{n+1}\pi$, where $k = 1, 2, ..., n$ is the index number of kth splitting valence band. In the bulk limit ($n \to \infty$), the eigenvalue of the Γ point is expected to be $E_{1\nu} + 2J_\nu = -3.16$ eV with respect to the vacuum level. In other words, compared with the monolayer, the gap value of bulk black phosphorus reduces at least 0.88 eV if one also considers the evolution of CBE toward the Fermi level. This prediction agrees well with our previous DFT-PBE results.[27]

Overall, the SEIC model results are in good agreement with those obtained from DFT, as shown in Figures 8 and 9. However, the SEIC model predicts that the VBEs of the quadrilayer or more-layer systems along the Γ−Y direction still remain quadratic-like shaped, instead of showing the linear-like shape from DFT calculations (see Figure 9c and d). This disagreement is probably caused by the negligence of the stronger coupling between the VBE and CBE when they get close in the quadrilayer or thicker systems. However, it should be emphasized here that the artificial linear dispersion of the quadrilayer is derived from the problem of the band gap underestimation related to the local or semilocal approximations of the exchange−correlation functional in DFT. On the basis of the first-order $\mathbf{k}\cdot\mathbf{p}$ perturbation theory,[57] we use a degenerate two-band model to describe the coupling between the valence and conduction bands for these systems. Our results indicate that this coupling does lead to the linear-dominated dispersion along the armchair direction and the quadratic-dominated dispersion along the zigzag direction, respectively.

We expect that our SEIC model is also applicable to the evolution of the CBE. Note that the evolution of the CBE is different from that of the VBE, as an illustrative example, we choose the case of the trilayer system; one can observe in Figure 8c that the energies of the second and third conduction bands near the Γ point become very close to each other, while the second and third valence bands are separated by an energy of $\sqrt{2}J_\nu(k_x, k_y)$ eV. This means the coupling among s, p_y, and p_z becomes noticeable and cannot be neglected. Further calculations show that the relative positions of the first four conduction bands at the Γ point can be qualitatively determined if we include the s and p_y states into the SEIC model to describe the evolution of the CBE. Previous theoretical studies suggested that the decreasing tendency of the band gap with increasing film thickness is likely an outcome of the quantum confinement effect.[15,26] We argue that it would be sufficient to explain such an observed tendency using a simple SEIC model. Clearly, the dramatic decrease of hole mass is also attributed to interlayer coupling. We hope that this systematic study serves as a guideline for the interpretation of the evolution of band edges in other two-dimensional layered materials.

To conclude, through first-principles calculations and a SEIC model, we have uncovered the nature and evolution of the valence band edge as a function of the number of P layers in few-layer phosphorene. Our results predict that the interlayer

DOI: 10.1021/acs.jpclett.5b02047
J. Phys. Chem. Lett. 2015, 6, 4876−4883

coupling plays a vital role in determining the decreasing trend for both band gap and carrier effective masses with the increase of phosphorene thickness. Also, the interlayer coupling leads to a transition from indirect to direct when changing from monolayer to few-layer phosphorene. The analysis of the orbital-decomposed band structure reveals that the upward shift of the VBM is faster than that of the CBM due to the larger contribution of p_z in the former.

■ ASSOCIATED CONTENT

Supporting Information

The Supporting Information is available free of charge on the ACS Publications website at DOI: 10.1021/acs.jpclett.5b02047.

HSE06-calculated band edges of quadrilayer phosphorene and bulk black phosphorous along the Γ−Y direction; PBE-calculated global evolution of both VBE and CBE for few-layer quadrilayer phosphorene (PDF)

■ AUTHOR INFORMATION

Corresponding Authors

*E-mail: wangvei@icloud.com (V.W.).
*E-mail: geng@ustb.edu.cn (W.T.G.).

Notes

The authors declare no competing financial interest.

■ ACKNOWLEDGMENTS

We acknowledge the financial support of the Special Scientific Research Program of the Education Bureau of Shaanxi Province, China (Grant No. 15JK1531), the National Natural Science Foundation of Special Theoretical Physics (Grant No. 11447217), and the National Natural Science Foundation of China (Grant Nos. 11304245, 11304244, and 61308006). Y.K. is thankful to the Russian Megagrant Project No. 14.B25.31.0030 "New energy technologies and energy carriers" for supporting the present research. The calculations were performed on the HITACHI SR16000 supercomputer at the Institute for Materials Research of Tohoku University, Japan.

■ REFERENCES

(1) Li, L.; Yu, Y.; Ye, G. J.; Ge, Q.; Ou, X.; Wu, H.; Feng, D.; Chen, X. H.; Zhang, Y. Black Phosphorus Field-Effect Transistors. *Nat. Nanotechnol.* **2014**, *9*, 372−377.

(2) Liu, H.; Neal, A. T.; Zhu, Z.; Luo, Z.; Xu, X.; Tománek, D.; Ye, P. D. Phosphorene: An Unexplored 2D Semiconductor with a High Hole Mobility. *ACS Nano* **2014**, *8*, 4033−4041.

(3) Dai, J.; Zeng, X. C. Bilayer Phosphorene: Effect of Stacking Order on Bandgap and Its Potential Applications in Thin-Film Solar Cells. *J. Phys. Chem. Lett.* **2014**, *5*, 1289−1293.

(4) Koenig, S. P.; Doganov, R. A.; Schmidt, H.; Castro Neto, A. H.; Oezyilmaz, B. Electric Field Effect in Ultrathin Black Phosphorus. *Appl. Phys. Lett.* **2014**, *104*, 103106.

(5) Ling, X.; Wang, H.; Huang, S.; Xia, F.; Dresselhaus, M. S. The Renaissance of Black Phosphorus. *Proc. Natl. Acad. Sci. U. S. A.* **2015**, *112*, 4523−4530.

(6) Qiao, J.; Kong, X.; Hu, Z.-X.; Yang, F.; Ji, W. High-Mobility Transport Anisotropy and Linear Dichroism in Few-Layer Black Phosphorus. *Nat. Commun.* **2014**, *5*, 4475.

(7) Wang, X.; Jones, A. M.; Seyler, K. L.; Tran, V.; Jia, Y.; Zhao, H.; Wang, H.; Yang, L.; Xu, X.; Xia, F. Highly Anisotropic and Robust Excitons in Monolayer Black Phosphorus. *Nat. Nanotechnol.* **2015**, *10*, 517−521.

(8) Yuan, H.; Liu, X.; Afshinmanesh, F.; Li, W.; Xu, G.; Sun, J.; Lian, B.; Curto, A. G.; Ye, G.; Hikita, Y.; et al. Polarization-Sensitive Broadband Photodetector using a Black Phosphorus Vertical p-n Junction. *Nat. Nanotechnol.* **2015**, *10*, 707−713.

(9) Keyes, R. W. The Electrical Properties of Black Phosphorus. *Phys. Rev.* **1953**, *92*, 580.

(10) Brown, A.; Rundqvist, S. Refinement of the Crystal Structure of Black Phosphorus. *Acta Crystallogr.* **1965**, *19*, 684−685.

(11) Maruyama, Y.; Suzuki, S.; Kobayashi, K.; Tanuma, S. Synthesis and Some Properties of Black Phosphorus Single Crystals. *Physica B+C* **1981**, *105*, 99−102.

(12) Akahama, Y.; Endo, S.; Narita, S.-i. Electrical Properties of Black Phosphorus Single Crystals. *J. Phys. Soc. Jpn.* **1983**, *52*, 2148−2155.

(13) Asahina, H.; Morita, A. Band Structure and Optical Properties of Black Phosphorus. *J. Phys. C: Solid State Phys.* **1984**, *17*, 1839.

(14) Zhang, S.; Yang, J.; Xu, R.; Wang, F.; Li, W.; Ghufran, M.; Zhang, Y.-W.; Yu, Z.; Zhang, G.; Qin, Q.; et al. Extraordinary Photoluminescence and Strong Temperature/Angle-Dependent Raman Responses in Few-Layer Phosphorene. *ACS Nano* **2014**, *8*, 9590−9596.

(15) Tran, V.; Soklaski, R.; Liang, Y.; Yang, L. Layer-Controlled Band Gap and Anisotropic Excitons in Few-Layer Black Phosphorus. *Phys. Rev. B: Condens. Matter Mater. Phys.* **2014**, *89*, 235319.

(16) Peng, X.; Wei, Q.; Copple, A. Strain-Engineered Direct-Indirect Band Gap Transition and Its Mechanism in Two-Dimensional Phosphorene. *Phys. Rev. B: Condens. Matter Mater. Phys.* **2014**, *90*, 085402.

(17) Liu, H.; Du, Y.; Deng, Y.; Ye, P. D. Semiconducting Black Phosphorus: Synthesis, Transport Properties and Electronic Applications. *Chem. Soc. Rev.* **2015**, *44*, 2732−2743.

(18) Xia, F.; Wang, H.; Jia, Y. Rediscovering Black Phosphorus as an Anisotropic Layered Material for Optoelectronics and Electronics. *Nat. Commun.* **2014**, *5*, 4458.

(19) Low, T.; Rodin, A. S.; Carvalho, A.; Jiang, Y.; Wang, H.; Xia, F.; Castro Neto, A. H. Tunable Optical Properties of Multilayer Black Phosphorus Thin Films. *Phys. Rev. B: Condens. Matter Mater. Phys.* **2014**, *90*, 075434.

(20) Low, T.; Roldán, R.; Wang, H.; Xia, F.; Avouris, P.; Moreno, L. M.; Guinea, F. Plasmons and Screening in Monolayer and Multilayer Black Phosphorus. *Phys. Rev. Lett.* **2014**, *113*, 106802.

(21) Rodin, A. S.; Carvalho, A.; Castro Neto, A. H. Strain-Induced Gap Modification in Black Phosphorus. *Phys. Rev. Lett.* **2014**, *112*, 176801.

(22) Li, P.; Appelbaum, I. Electrons and Holes in Phosphorene. *Phys. Rev. B: Condens. Matter Mater. Phys.* **2014**, *90*, 115439.

(23) Rudenko, A. N.; Yuan, S.; Katsnelson, M. I. Toward a Realistic Description of Multilayer Black Phosphorus: From *GW* Approximation to Large-Scale Tight-Binding Simulations. *Phys. Rev. B: Condens. Matter Mater. Phys.* **2015**, *92*, 085419.

(24) Ganesan, V. D. S.; Zhang, C.; Feng, Y. P.; Shen, L. Phosphorene and Transition Metal Dichalcogenide 2D Heterojunctions: Application in Excitonic Solar Cells. *arXiv:1507.07343* **2015**.

(25) Ziletti, A.; Huang, S. M.; Coker, D. F.; Lin, H. Van Hove Singularity and Ferromagnetic Instability in Phosphorene. *Phys. Rev. B: Condens. Matter Mater. Phys.* **2015**, *92*, 085423.

(26) Cai, Y.; Zhang, G.; Zhang, Y.-W. Layer-Dependent Band Alignment and Work Function of Few-Layer Phosphorene. *Sci. Rep.* **2014**, *4*, 6677.

(27) Wang, V.; Kawazoe, Y.; Geng, W. T. Native Point Defects in Few-Layer Phosphorene. *Phys. Rev. B: Condens. Matter Mater. Phys.* **2015**, *91*, 045433.

(28) Hohenberg, P.; Kohn, W. Inhomogeneous Electron Gas. *Phys. Rev.* **1964**, *136*, B864−B871.

(29) Kohn, W.; Sham, L. J. Self-Consistent Equations Including Exchange and Correlation Effects. *Phys. Rev.* **1965**, *140*, A1133−A1138.

(30) Kresse, G.; Furthmüller, J. Efficient Iterative Schemes for Ab Initio Total-Energy Calculations Using a Plane-Wave Basis Set. *Phys. Rev. B: Condens. Matter Mater. Phys.* **1996**, *54*, 11169−11186.

DOI: 10.1021/acs.jpclett.5b02047
J. Phys. Chem. Lett. 2015, 6, 4876−4883

(31) Kresse, G.; Furthmüller, J. Efficiency of Ab-Initio Total Energy Calculations for Metals and Semiconductors Using a Plane-Wave Basis Set. *Comput. Mater. Sci.* **1996**, *6*, 15−50.
(32) Blöchl, P. E. Projector Augmented-Wave Method. *Phys. Rev. B: Condens. Matter Mater. Phys.* **1994**, *50*, 17953−17979.
(33) Kresse, G.; Joubert, D. From Ultrasoft Pseudopotentials to the Projector Augmented-Wave Method. *Phys. Rev. B: Condens. Matter Mater. Phys.* **1999**, *59*, 1758−1775.
(34) Perdew, J. P.; Burke, K.; Ernzerhof, M. Generalized Gradient Approximation Made Simple. *Phys. Rev. Lett.* **1996**, *77*, 3865−3868.
(35) Appalakondaiah, S.; Vaitheeswaran, G.; Lebegue, S.; Christensen, N. E.; Svane, A. Effect of van der Waals Interactions on the Structural and Elastic Properties of Black Phosphorus. *Phys. Rev. B: Condens. Matter Mater. Phys.* **2012**, *86*, 035105.
(36) Grimme, S. Semiempirical GGA-type Density Functional Constructed with a Long-Range Dispersion Correction. *J. Comput. Chem.* **2006**, *27*, 1787−1799.
(37) Bučko, T.; Hafner, J.; Lebègue, S.; Ángyán, J. Improved Description of the Structure of Molecular and Layered Crystals: Ab Initio DFT Calculations with van der Waals Corrections. *J. Phys. Chem. A* **2010**, *114*, 11814−11824.
(38) Perdew, J. P.; Zunger, A. Self-Interaction Correction to Density-Functional Approximations for Many-Electron Systems. *Phys. Rev. B: Condens. Matter Mater. Phys.* **1981**, *23*, 5048−5079.
(39) Perdew, J. P.; Ernzerhof, M.; Burke, K. Rationale for Mixing Exact Exchange with Density Functional Approximations. *J. Chem. Phys.* **1996**, *105*, 9982−9985.
(40) Paier, J.; Marsman, M.; Hummer, K.; Kresse, G.; Gerber, I. C.; Angyan, J. G. Screened Hybrid Density Functionals Applied to Solids. *J. Chem. Phys.* **2006**, *124*, 154709.
(41) Marsman, M.; Paier, J.; Stroppa, A.; Kresse, G. Hybrid Functionals Applied to Extended Systems. *J. Phys.: Condens. Matter* **2008**, *20*, 064201.
(42) Mostofi, A. A.; Yates, J. R.; Lee, Y.-S.; Souza, I.; Vanderbilt, D.; Marzari, N. Wannier90: a Tool for Obtaining Maximally-Localised Wannier Functions. *Comput. Phys. Commun.* **2008**, *178*, 685−699.
(43) Heyd, J.; Scuseria, G. E.; Ernzerhof, M. Hybrid Functionals Based on a Screened Coulomb Potential. *J. Chem. Phys.* **2003**, *118*, 8207−8215.
(44) Krukau, A. V.; Vydrov, O. A.; Izmaylov, A. F.; Scuseria, G. E. Influence of the Exchange Screening Parameter on the Performance of Screened Hybrid Functionals. *J. Chem. Phys.* **2006**, *125*, 224106.
(45) Monkhorst, H. J.; Pack, J. D. Special Points for Brillouin-Zone Integrations. *Phys. Rev. B* **1976**, *13*, 5188−5192.
(46) Wang, V. VASPKIT, a Post-Processing Program for the VASP Code. http://vaspkit.sourceforge.net (2013).
(47) Komsa, H.-P.; Krasheninnikov, A. V. Effects of Confinement and Environment on the Electronic Structure and Exciton Binding Energy of MoS_2 from First Principles. *Phys. Rev. B: Condens. Matter Mater. Phys.* **2012**, *86*, 241201.
(48) Bhandari, C.; Lambrecht, W. R. L.; van Schilfgaarde, M. Quasiparticle Self-Consistent *GW* Calculations of the Electronic Band Structure of Bulk and Monolayer V_2O_5. *Phys. Rev. B: Condens. Matter Mater. Phys.* **2015**, *91*, 125116.
(49) Çak ır, D.; Sahin, H.; Peeters, F. m. c. M. Tuning of the Electronic and Optical Properties of Single-Layer Black Phosphorus by Strain. *Phys. Rev. B: Condens. Matter Mater. Phys.* **2014**, *90*, 205421.
(50) Seixas, L.; Rodin, A. S.; Carvalho, A.; Castro Neto, A. H. Exciton Binding Energies and Luminescence of Phosphorene under Pressure. *Phys. Rev. B: Condens. Matter Mater. Phys.* **2015**, *91*, 115437.
(51) Kim, J.; Baik, S. S.; Ryu, S. H.; Sohn, Y.; Park, S.; Park, B.-G.; Denlinger, J.; Yi, Y.; Choi, H. J.; Kim, K. S. Observation of Tunable Band Gap and Anisotropic Dirac Semimetal State in Black Phosphorus. *Science* **2015**, *349*, 723−726.
(52) Liu, Q.; Zhang, X.; Abdalla, L. B.; Fazzio, A.; Zunger, A. Switching a Normal Insulator into a Topological Insulator via Electric Field with Application to Phosphorene. *Nano Lett.* **2015**, *15*, 1222−1228.
(53) Fei, R.; Tran, V.; Yang, L. Topologically Protected Dirac Cones in Compressed Bulk Black Phosphorus. *Phys. Rev. B: Condens. Matter Mater. Phys.* **2015**, *91*, 195319.
(54) Dolui, K.; Quek, S. Y. Quantum-Confinement and Structural Anisotropy Result in Electrically-Tunable Dirac Cone in Few-layer Black Phosphorous. *Sci. Rep.* **2015**, *5*, 11699.
(55) Padilha, J. E.; Peelaers, H.; Janotti, A.; van de Walle, C. G. Nature and Evolution of the Band-Edge States in MoS_2: From Monolayer to Bulk. *Phys. Rev. B: Condens. Matter Mater. Phys.* **2014**, *90*, 205420.
(56) Yates, K. *Hückel Molecular Orbital Theory*; Elsevier Academic Press: New York, 1978.
(57) Dresselhaus, M. S.; Dresselhaus, G.; Jorio, A. *Group Theory: Application to the Physics of Condensed Matter*; Springer: Berlin, Germany, 2007.

DOI: 10.1021/acs.jpclett.5b02047
J. Phys. Chem. Lett. 2015, 6, 4876−4883